Carbohydrate Polymers 91 (2013) 543–548

Contents lists available at SciVerse ScienceDirect

Carbohydrate Polymers

journal homepage: www.elsevier.com/locate/carbpol

Thermal expansion behavior of hydrate paramylon in the low-temperature region

Kayoko Kobayashi [a], Satoshi Kimura [a,b], Eiji Togawa [c], Masahisa Wada [a,b,*]

[a] Department of Biomaterials Science, Graduate School of Agricultural and Life Sciences, The University of Tokyo, Tokyo 113-8657, Japan
[b] Department of Plant & Environmental New Resources, College of Life Sciences, Kyung Hee University, 1 Seocheon-dong, Giheung-ku, Yongin-si, Gyeonggi-do 446-701, Republic of Korea
[c] Forestry and Forest Products Research Institute, Matsunosato 1, Tsukuba, Ibaraki 305-8687, Japan

ARTICLE INFO

Article history:
Received 9 May 2012
Received in revised form 9 August 2012
Accepted 19 August 2012
Available online 24 August 2012

Keywords:
Paramylon
(1→3)-β-D-Glucan
Synchrotron X-ray powder diffraction
Solid-state ^{13}C NMR
Thermal expansion
Phase transition

ABSTRACT

The thermal expansion behavior of hydrate paramylon between 100 and 300 K has been investigated using synchrotron X-ray powder diffraction. The X-ray diffraction profile at 300 K showed a typical pattern of the hydrate triple helical (1→3)-β-D-glucan with a hexagonal unit cell (a = 15.782 Å and c = 18.580 Å). On cooling, the hydrate paramylon had converted to a "low-temperature phase" around 270 K. On passing through the phase transition, the a-axis and c-axis values decreased and increased, respectively, and the low-temperature phase at 100 K exhibited a hexagonal unit cell (a = 15.586 Å and c = 18.619 Å). The phase transition took place reversibly. Below the transition point, both the a-axis and c-axis values decreased linearly. The thermal expansion coefficients are: $\alpha_a = 1.50 \times 10^{-5}\ K^{-1}$, $\alpha_c = 0.33 \times 10^{-5}\ K^{-1}$, and $\beta = 3.08 \times 10^{-5}\ K^{-1}$.

1. Introduction

(1→3)-β-D-Glucan is an abundant polysaccharide that is found in many organisms, such as bacteria, fungi, algae, and plants. Since most of these polysaccharides have branches through β-(1→6) linkages and/or include other linkages, such as β-(1→4) linkages, there are only a few known examples of (1→3)-β-D-glucan as linear homopolymers (Stone & Clarke, 1992), and among these, two well-known linear homopolymers of (1→3)-β-D-glucan, curdlan and paramylon (Clarke & Stone, 1960; Harada, Misaki, & Saito, 1968), have been used mainly for structural analysis of (1→3)-β-D-glucan. The crystal structure of (1→3)-β-D-glucan is of importance in medicine because its characteristic higher-order structure is considered to be a possible cause of its immunomodulation and antitumor activity (Ohno, Miura, Chiba, Adachi, & Yadomae, 1995; Yanaki, Itoh, & Tabata, 1986; Zhang, Li, Xu, & Zeng, 2005).

Paramylon is a storage granule that occurs in *Euglena* cells. Its most distinctive feature is its high degree of crystallinity, even though it serves as a storage carbohydrate (Booy, Chanzy, & Boudet, 1981; Chuah, Sarko, Deslandes, & Marchessault, 1983; Kiss, Roberts, Brown, & Triemer, 1988; Kobayashi, Kimura, Togawa, Wada, & Kuga, 2010; Marchessault & Deslandes, 1979). On the other hand, curdlan, the extracellular polysaccharide of *Alcaligenes* bacteria, has a lower degree of crystallinity. Thus, the full crystal structure of curdlan without any treatment is still to be determined, although two different models, the 7/1 triple helix and the 6/1 single helix structure, have been proposed in several studies (Okuyama et al., 1991; Stipanovic & Giammatteo, 1987; Takeda, Yasuoka, Kasai, & Harada, 1978). However, on annealing, curdlan is converted to another crystalline form with a higher degree of crystallinity. This crystalline form of annealed curdlan is the same as that of paramylon, and there are both hydrate and anhydrous forms (Marchessault & Deslandes, 1979; Marchessault, Deslandes, Ogawa, & Sundararajan, 1977).

Triple helical models have been proposed using a combination of X-ray diffraction analysis and stereochemical modeling for both the hydrate and anhydrous forms (Chuah et al., 1983; Deslandes, Marchessault, & Sarko, 1980). In the model of the anhydrous form (Fig. 1) (Deslandes et al., 1980), the 6/1 triple helices are packed in a hexagonal unit cell (a = 14.41 Å, c = 5.87 Å). All the glucan chains are arranged in a parallel manner, and the space group is $P6_3$. On the other hand, in the hydrate form (Chuah et al., 1983), the similar triple helices are also arranged in a hexagonal unit cell (a = 15.56 Å, c = 18.78 Å), but water molecules are located between the triple helices, resulting in a longer a-axis value than in the anhydrous

* Corresponding author at: Department of Biomaterials Science, Graduate School of Agricultural and Life Sciences, The University of Tokyo, Tokyo 113-8657, Japan. Tel.: +81 3 5841 5247; fax: +81 3 5841 2677.
E-mail address: awadam@mail.ecc.u-tokyo.ac.jp (M. Wada).

0144-8617/$ – see front matter © 2012 Elsevier Ltd. All rights reserved.
http://dx.doi.org/10.1016/j.carbpol.2012.08.067

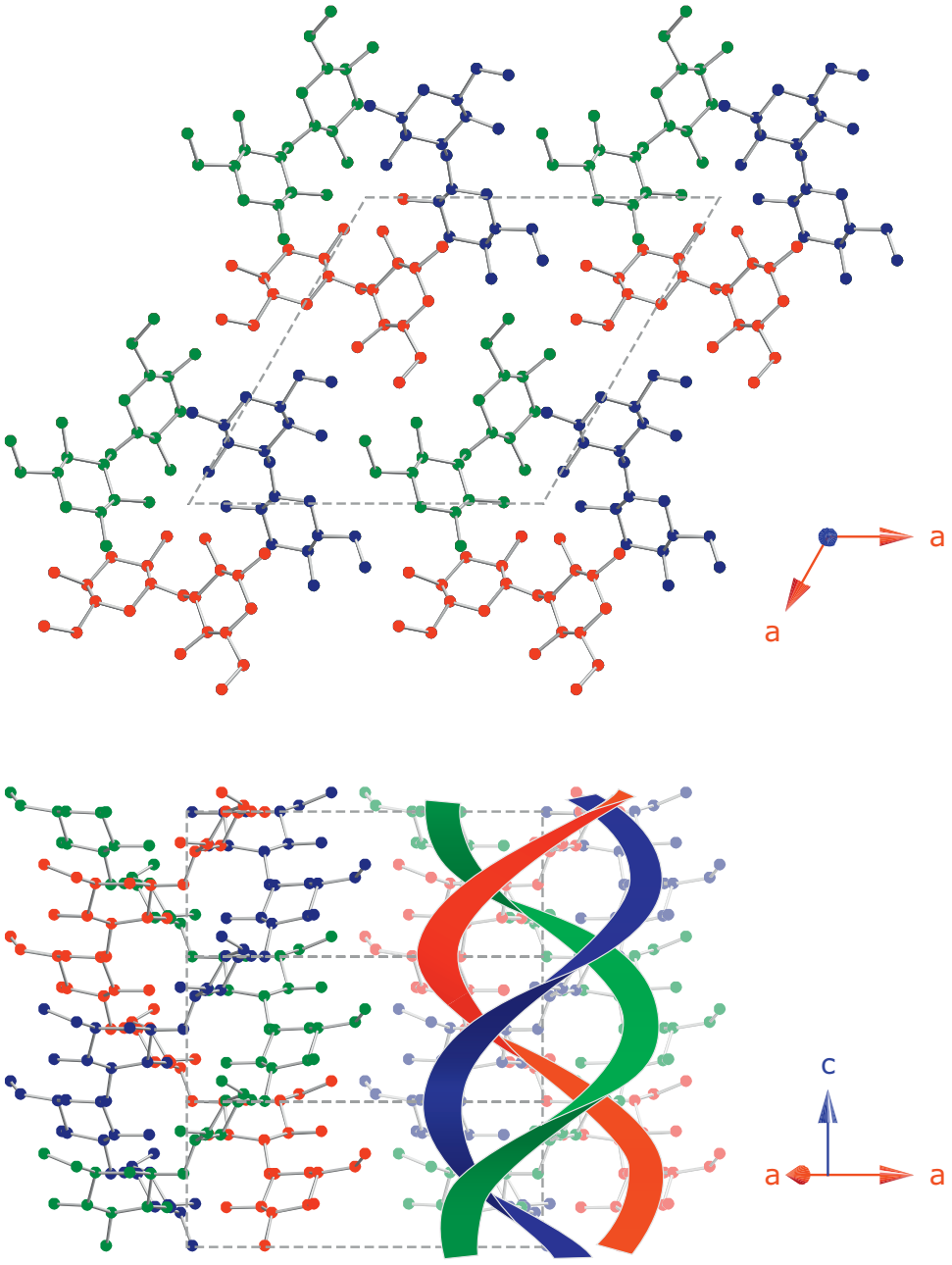

Fig. 1. The triple helical model of anhydrous (1→3)-β-D-glucan proposed by Deslandes et al. (1980).

form. Furthermore, the hydrate form has lower symmetry. The *c*-axis length corresponds to the pitch of the 6/1 helices, which is three times longer than the pitch of the anhydrous form, and its space group is *P*1.

Since paramylon is a granular material, oriented samples cannot be prepared, which is a crucial disadvantage for structural analysis. In previous X-ray diffraction studies (Chuah et al., 1983; Deslandes et al., 1980), paramylon was only studied to complement the fiber diffraction data of annealed curdlan to determine the hydrate form (Chuah et al., 1983). However, we found that never-dried paramylon had a high degree of crystallinity, because the degree of crystallinity decreased on passing through the transition between the hydrate and anhydrous forms (Kobayashi et al., 2010). X-ray diffractometry on never-dried paramylon provided a resolution of 1.5 Å, and the crystallite size calculated using the Scherrer equation was >40 nm. Further analysis on paramylon samples that showed such a high resolution would help us to revisit the crystal structure of (1→3)-β-D-glucan. In this study, we carried out synchrotron X-ray powder diffraction measurements on never-dried samples to obtain diffraction data of hydrate paramylon with a higher resolution.

Furthermore, we carried out the X-ray diffraction measurements from 300 to 100 K to observe the thermal expansion behavior in the low-temperature region. An understanding of the thermal expansion properties would lead to a better understanding of the crystal structure because they are closely related to each other, and an understanding of the thermal stability is also significant for practical applications. The thermal expansion behavior of many major

natural polysaccharides, such as cellulose (Hidaka, Kim, & Wada, 2010; Hori & Wada, 2006; Wada, 2002; Wada, Kwon, & Nishiyama, 2008; Wada, Hori, Kim, & Sasaki, 2010), amylose (Nishiyama, Putaux, Montesanti, Hazemann, & Rochas, 2010), chitin (Ogawa, Hori, Kim, & Wada, 2011; Wada & Saito, 2001), and mannan (Hori, Sugiyama, & Wada, 2007), has been studied, but the thermal expansion behavior of triple helical (1→3)-β-D-glucan is still not known. In our thermal expansion experiments, we found that a phase transition took place at low temperatures. Thus, we will also report on a new "low-temperature phase" of hydrate paramylon in this work.

2. Experimental

2.1. Cultivation of euglena and preparation of the paramylon samples

Euglena gracilis NIES-48 was cultured, and paramylon samples were prepared from the cultured cells, as reported previously (Kobayashi et al., 2010). The purified samples were stored in deionized water or at a relative humidity of RH = 85% in a desiccator over a saturated KCl solution.

2.2. Synchrotron X-ray powder diffraction measurements

Synchrotron X-ray powder diffraction measurements were carried out using the BL02B2 beam line located at the SPring-8 facility (Hyogo, Japan). A paramylon sample stored at RH = 85% was sealed in a glass capillary and placed on a large Debye–Scherrer camera. The X-ray wavelength used was 0.99746(2) Å, which was calibrated using the lattice constants of CeO_2. The data were recorded on an imaging plate at temperatures between 300 and 100 K, controlled using a low-temperature nitrogen gas flow system. The exposure time for each measurement was 5 min.

The peak positions in the obtained profiles were determined using a peak-fitting procedure employing a nonlinear least-squares method, as reported previously (Wada, Okano, & Sugiyama, 1997). Accurate *d*-spacing values were calculated from the peak positions, and the unit cell parameters were determined from the *d*-spacing values and the indices using a nonlinear least-squares method. The linear and volumetric thermal expansion coefficients, α and β, respectively, were determined using the following equations:

$$\alpha = \frac{1}{l_{t=0}} \times \frac{\Delta l}{\Delta t}$$

$$\beta = \frac{1}{V_{t=0}} \times \frac{\Delta V}{\Delta t}$$

where l is a unit cell parameter, V is the unit cell volume, and t is the temperature (K).

2.3. Solid-state CP/MAS ^{13}C NMR spectroscopy

Solid-state ^{13}C NMR spectra of the samples in a wet condition were obtained using a CMX 300 spectrometer (Chemagnetics, USA) operating at 75.6 MHz. The measurements were performed at 298 and 245 K. Before measurements were performed on the samples, the sample temperatures were verified using the ^{207}Pb NMR resonance of solid $Pb(NO_3)_2$ for calibration. The sample in a 4.0 mm zirconia rotor was spun at 5 kHz in a solid-state probe at the magic angle. All spectra were obtained using ^{1}H NMR 90° pulse lengths of 2.5 μs, with a cross-polarization time of 1.0 ms and a 60 kHz CW proton decoupling. The recycle time was 3 s. The spectra were calibrated using adamantane as a standard. The rotor was sealed by a Teflon cap to avoid any drying of the samples.

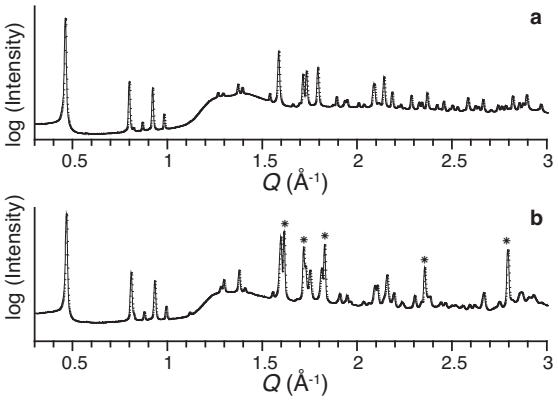

Fig. 2. Synchrotron X-ray diffraction profiles of hydrate paramylon obtained at: (a) 300 K and (b) 100 K. The peaks indicated by an asterisk (*) are derived from ice crystals (ice Ih). The term Q is the scattering vector ($2\pi/d$).

3. Results and discussion

3.1. Synchrotron X-ray powder diffraction of hydrate paramylon at 300 and 100 K

X-ray diffraction measurements were carried out on hydrate paramylon at 300 and 100 K, and both profiles are shown in Fig. 2. Although several diffraction patterns at room temperature, i.e. at approximately 300 K, have been reported previously, and they show exceptionally high resolution for natural polysaccharides (Chuah et al., 1983; Kiss et al., 1988; Kobayashi et al., 2010; Marchessault & Deslandes, 1979), the data obtained at 300 K in this study had an even better resolution (Fig. 2(a)). The peaks were extremely sharp, which enabled the separation of some peaks occurring close together that were observed up to the high Q region. In addition, weak intensity peaks that had not been observed so far, such as the small peak occurring at $Q = 0.82$ Å^{-1}, were also observed. However, all the observed peaks could be indexed according to the hexagonal unit cell, as reported previously, and the unit cell parameters were determined to be: $a = 15.782(2)$ Å and $c = 18.580(2)$ Å. These values are close to the values found in previous studies (Chuah et al., 1983; Kobayashi et al., 2010).

The profile obtained at 100 K was similar to that at 300 K, but there were different features in the profile (Fig. 2(b)). The strong and sharp peaks, which did not appear in the profile at 300 K, were observed over $Q = 1.6$ Å^{-1}, and all the peaks were indexed according to the hexagonal ice (Ice Ih) (Röttger, Endriss, Ihringer, Doyle, & Kuhs, 1994). The intensity ratio appeared to change, which was particularly prominent for $Q = 1$–1.5 Å^{-1}, and most of the peaks were shifted slightly to a higher Q region. In addition, each peak was broadened, resulting in a decrease in resolution. This result indicated that the high degree of crystallinity of hydrate paramylon had decreased on cooling to 100 K. The unit cell parameters at 100 K were calculated assuming a hexagonal unit cell, and they were determined to be: $a = 15.586(6)$ Å and $c = 18.619(7)$ Å. Compared with the values found at 300 K, the a-axis value had decreased by 1.2%, whereas the c-axis length had increased by 0.2%.

3.2. Thermal expansion behavior of hydrate paramylon from 300 to 100 K

The cooling of hydrate paramylon from 300 to 100 K was monitored using synchrotron X-ray powder diffraction using a stepwise decrease of 25 K. The unit cell parameters and volume at each temperature were calculated and are shown in Fig. 3.

The thermal expansion behavior of hydrate paramylon from 300 to 100 K appeared to be divided into two parts: above and

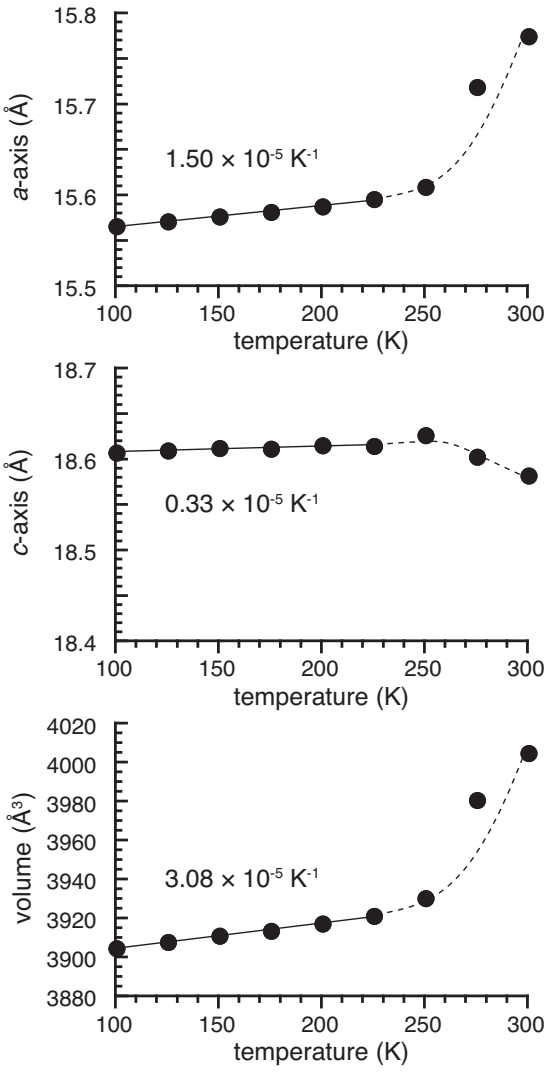

Fig. 3. Changes in the unit cell parameter and volume of hydrate paramylon on cooling from 300 to 100 K. The values of the thermal expansion coefficients are also given.

below 250 K. From 300 to 250 K, the diffraction pattern changed from that typically observed at room temperature, as shown in Fig. 1(a), to that observed in the low-temperature region, as shown in Fig. 1(b). At the same time, the unit cell parameters and volume showed marked changes: a marked decrease in the *a*-axis length and the unit cell volume, and a slight increase in the *c*-axis length (Fig. 3). On the other hand, below 250 K, there were no significant changes observed in the diffraction patterns, which were the same as that shown in Fig. 1(b). Any changes in the unit cell parameters and volume were also very small in this temperature region, and they decreased almost linearly with further cooling (Fig. 3). These results indicated that the thermal expansion from 300 to 100 K was not a continuous process, and that a phase transition occurred in the region 250–300 K. In addition to the "room-temperature (RT) phase" that has been observed so far for hydrate paramylon, there is another phase of hydrate paramylon, a "low-temperature (LT) phase." Once the hydrate paramylon is converted to the LT phase, it is stable down to a temperature of at least 100 K. A similar phase transition induced by temperature change has also been reported for another polysaccharide, cellulose I_β, in the high-temperature region (Wada et al., 2010).

In the LT phase of hydrate paramylon, the thermal expansion coefficients were calculated to be $\alpha_a = 1.50 \times 10^{-5}\,K^{-1}$, $\alpha_c = 0.33 \times 10^{-5}\,K^{-1}$, and $\beta = 3.08 \times 10^{-5}\,K^{-1}$. The value of α_a is about five times larger than that of α_c, which indicates that the distance between the triple helices had contracted a large distance, but the pitch of the triple helices did not contract much on cooling to the LT phase of hydrate paramylon. These absolute values do not differ greatly from those of other polysaccharides (Hidaka et al., 2010; Hori & Wada, 2006; Hori et al., 2007; Ogawa et al., 2011; Wada & Saito, 2001; Wada et al., 2010; Wada, 2002). However, the value of the chain axis direction, α_c, was even smaller than the corresponding values of cellulose and chitin (Hidaka et al., 2010; Ogawa et al., 2011), which have an extended chain conformation. The value of α_c was positive, whereas the similar values of A- and B-amylose, which have a double helical structure, are negative (Nishiyama et al., 2010).

3.3. Transition between the room-temperature phase and the low-temperature phase of hydrate paramylon

Further analysis in the temperature region where the phase transition occurs was carried out. The cooling and subsequent heating between 300 and 240 K were monitored using a stepwise decrease or increase in temperature of 10 K. The changes in the calculated unit cell parameters and volumes are shown in Fig. 4.

During cooling, the diffraction patterns of the RT phase (Fig. 1(a)) changed to that typical of the LT phase (Fig. 1(b)), in part, at 270 K, and this change was complete at 260 K. During subsequent heating, the diffraction patterns of the LT phase (Fig. 1(b)) returned to that observed for the RT phase (Fig. 1(a)) at 270–280 K. This phase transition occurred reversibly, with a transition point occurring at about 270 K. On passing through the phase transition, the unit cell parameters and volume changed rapidly (Fig. 4). The *a*-axis length and unit cell volume decreased and increased on passing through the transition from the RT phase to the LT phase and in the reverse direction, respectively. In contrast, the *c*-axis length increased and decreased on passing through the transition from the RT phase to the LT phase and in the reverse direction, respectively.

Interestingly, the transition point is close to the freezing point of water, and peaks from ice Ih appeared and disappeared at the point where the phase transition occurred. These ice Ih peaks were derived from a small volume of water that remained on the crystalline surface, although the samples had been stored at RH = 85% to remove any excess water. Our previous study implied that the volume of adsorbed water on the crystalline surface of paramylon would influence the crystal structure, because the value of the *a*-axis changed depending on the relative humidity (Kobayashi et al., 2010). However, in this study, the freezing and thawing of the adsorbed water had no apparent effect on the phase transition, because the diffraction profile at 280 K on heating showed ice peaks, but had completely converted to the RT phase (data not shown). Therefore, it remains unclear what causes the phase transition of hydrate paramylon near to the freezing point of water. Further analysis of other hydrate polysaccharides may provide useful information in understanding this phenomenon.

3.4. Solid-state ^{13}C NMR spectrum of the low-temperature phase of hydrate paramylon

Fig. 5 shows solid-state ^{13}C NMR spectra of the RT and LT phases recorded at 298 and 245 K, respectively. The spectrum of the RT phase was typical of hydrate paramylon, as reported previously (Fyfe et al., 1984; Kobayashi et al., 2010; Saito, Tabeta, Yokoi, & Erata, 1987; Saito, Yokoi, & Yoshioka, 1989). The peaks were very sharp, and the signals from the C3, C4, C5, and C6 atoms were split into several peaks, implying a low symmetry in the crystal structure. On converting to the LT phase, the spectrum also showed a

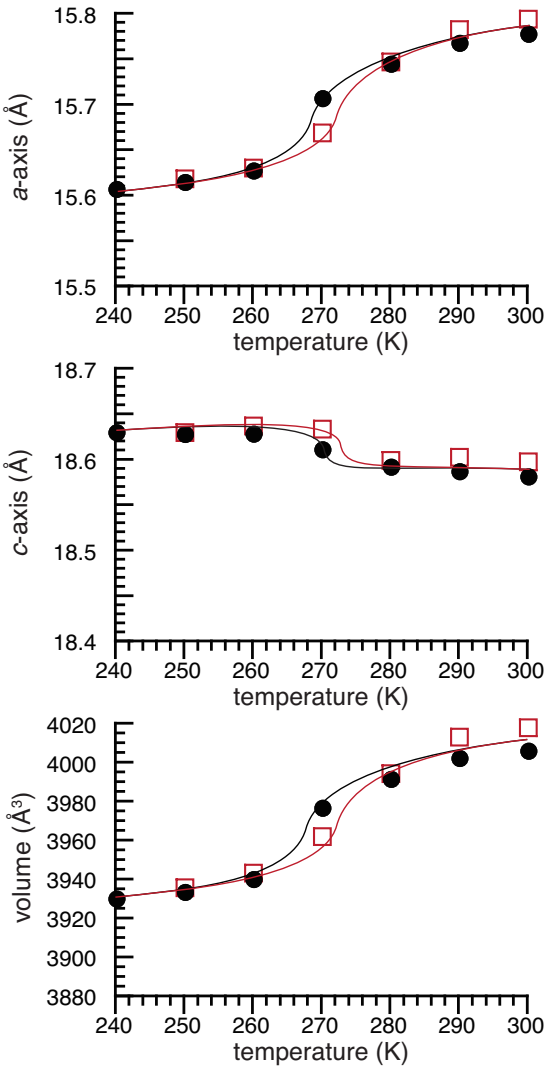

Fig. 4. Changes in the unit cell parameters and volume of hydrate paramylon on cooling from 300 to 240 K (filled circles) and subsequent heating from 240 to 300 K (open squares).

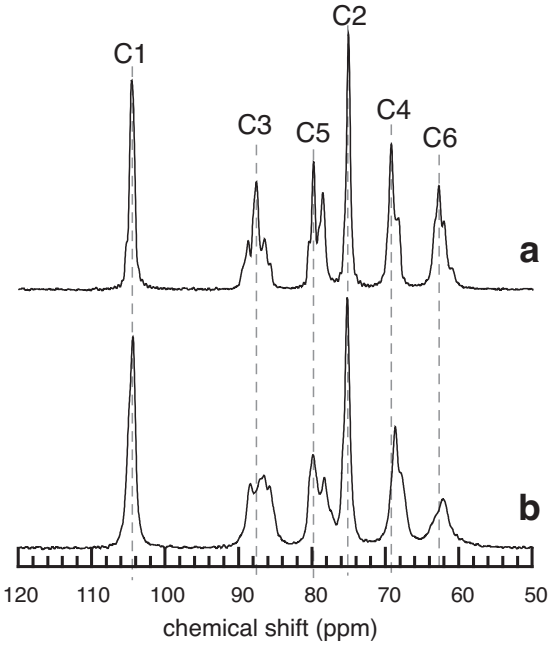

Fig. 5. Solid-state CP/MAS ^{13}C NMR spectra of hydrate paramylon: (a) RT phase obtained at 298 K and (b) LT phase obtained at 245 K.

complex pattern, but it became more difficult to distinguish one peak from another because the peaks became broader. The LT phase had a more disordered structure than the RT phase, which was consistent with the results of the X-ray diffraction analysis. Although the peak positions could not be determined for this reason, the peak positions of the C3, C4, and C6 atoms obviously changed, and the intensity distributions also changed significantly for the C3 and C6 atoms.

The structure of hydrate paramylon is not known in detail, but these results suggest that there are some differences between the structures of the RT and LT phases. In the triple helical structure (Fig. 1), the hydroxymethyl groups, corresponding to the C6 atoms, are located at the helix exterior, and play an important role in the hydrogen bonding scheme by forming hydrogen bonds with an adjacent triple helix or with water molecules (Chuah et al., 1983). Therefore, the conformational changes in the C6 atoms indicated that there was a marked change in the inter-helix hydrogen bonds via the water molecules, which resulted in the change in the *a*-axis length on passing through the phase transition. At the same time, the conformation of the glucan chains also changed, as indicated by the shift of the peaks from the C3 and C4 atoms. This is also supported by the results of the X-ray diffraction analysis, where the *c*-axis length also changed slightly on passing through the phase transition.

4. Conclusions

From our synchrotron X-ray powder diffraction analysis, we found that the crystal structure of hydrate paramylon, which had been observed at the room temperature (RT phase), exists at another phase in the low-temperature region (LT phase). The phase transition between the RT phase and the LT phase took place reversibly on cooling/heating around 270 K. On passing through the phase transition from the RT to the LT phase, the *a*-axis and *c*-axis values rapidly decreased and increased, respectively, and the X-ray diffraction profiles also showed some changes. In addition, solid-state ^{13}C NMR analysis indicated a conformational difference between the RT and LT phases. However, because the crystal structure of hydrate (1→3)-β-D-glucan is still not fully understood, the details of the changes that occur during the phase transition remain speculative. As shown in the ^{13}C NMR spectra, the crystal structure is complex, and therefore it will be difficult to determine the structure precisely. The powder diffraction data obtained in this study, which have the highest resolution obtained so far, are expected to lead to its elucidation in the future.

Acknowledgments

The synchrotron radiation experiments were performed at BL02B2 in SPring-8 with the approval of the Japan Synchrotron Research Institute (JASRI) (Proposal No. 2010B1247). This study was partly supported by a Grant-in-Aid for JSPS Fellows (23 2511).

References

Booy, F. P., Chanzy, H., & Boudet, A. (1981). An electron diffraction study of paramylon storage granules from *Euglena gracilis*. *Journal of Microscopy*, *121*, 133–140.
Chuah, C. T., Sarko, A., Deslandes, Y., & Marchessault, R. H. (1983). Triple-helical crystalline structure of curdlan and paramylon hydrates. *Macromolecules*, *16*, 1375–1382.

Clarke, A. E., & Stone, B. A. (1960). Structure of the paramylon from *Euglena gracilis*. *Biochimica et Biophysica Acta*, *44*, 161–163.
Deslandes, Y., Marchessault, R. H., & Sarko, A. (1980). Triple-helical structure of (1→3)-β-D-glucan. *Macromolecules*, *13*, 1466–1471.
Fyfe, C. A., Stephenson, P. J., Taylor, M. G., Bluhm, T. L., Deslandes, Y., & Marchessault, R. H. (1984). Hydration effects in the ^{13}C CP/MAS NMR spectra of solid (1→3)-β-D-glucans. *Macromolecules*, *17*, 501–502.
Harada, T., Misaki, A., & Saito, H. (1968). Curdlan: A bacterial gel-forming β-1,3-glucan. *Archives of Biochemistry and Biophysics*, *124*, 292–298.
Hidaka, H., Kim, U., & Wada, M. (2010). Synchrotron X-ray fiber diffraction study on the thermal expansion behavior of cellulose crystals in tension wood of Japanese poplar in the low-temperature region. *Holzforschung*, *64*, 167–171.
Hori, R., Sugiyama, J., & Wada, M. (2007). The thermal expansion of mannan I obtained from ivory nuts. *Carbohydrate Polymers*, *70*, 298–303.
Hori, R., & Wada, M. (2006). The thermal expansion of cellulose II and III_{II} crystals. *Cellulose*, *13*, 281–290.
Kiss, J. Z., Roberts, E. M., Brown, R. M., Jr., & Triemer, R. E. (1988). X-ray and dissolution studies of paramylon storage granules from *Euglena*. *Protoplasma*, *146*, 150–156.
Kobayashi, K., Kimura, S., Togawa, E., Wada, M., & Kuga, S. (2010). Crystal transition of paramylon with dehydration and hydration. *Carbohydrate Polymers*, *80*, 491–497.
Marchessault, R. H., & Deslandes, Y. (1979). Fine structure of (1→3)-β-D-glucans: Curdlan and paramylon. *Carbohydrate Research*, *75*, 231–242.
Marchessault, R. H., Deslandes, Y., Ogawa, K., & Sundararajan, P. R. (1977). X-ray diffraction data for β-(1→3)-D-glucan. *Canadian Journal of Chemistry*, *55*, 300–303.
Nishiyama, Y., Putaux, J.-L., Montesanti, N., Hazemann, J.-L., & Rochas, C. (2010). B→A allomorphic transition in native starch and amylose spherocrystals monitored by in situ synchrotron X-ray diffraction. *Biomacromolecules*, *11*, 76–87.
Ogawa, Y., Hori, R., Kim, U., & Wada, M. (2011). Elastic modulus in the crystalline region and the thermal expansion coefficients of α-chitin determined using synchrotron radiated X-ray diffraction. *Carbohydrate Polymers*, *83*, 1213–1217.
Ohno, N., Miura, N. N., Chiba, N., Adachi, Y., & Yadomae, T. (1995). Comparison of the immunopharmacological activities of triple and single-helical schizophyllan in mice. *Biological and Pharmaceutical Bulletin*, *18*, 1242–1247.
Okuyama, K., Otsubo, A., Fukuzawa, Y., Ozawa, M., Harada, T., & Kasai, N. (1991). Single-helical structure of native curdlan and its aggregation state. *Journal of Carbohydrate Chemistry*, *10*, 645–656.
Röttger, K., Endriss, A., Ihringer, J., Doyle, S., & Kuhs, W. F. (1994). Lattice constants and thermal expansion of H_2O and D_2O ice Ih between 10 and 265 K. *Acta Crystallographica Section B*, *50*, 644–648.
Saito, H., Tabeta, R., Yokoi, M., & Erata, T. (1987). A high-resolution solid-state ^{13}C NMR study of the secondary structure of linear (1→3)-β-D-glucans: A conformational elucidation of noncrystalline and crystalline forms by means of conformation-dependent ^{13}C chemical shifts. *Bulletin of the Chemical Society of Japan*, *60*, 4259–4266.
Saito, H., Yokoi, M., & Yoshioka, Y. (1989). Effect of hydration on conformational change or stabilization of (1→3)-β-D-glucans of various chain lengths in the solid state as studied by high-resolution solid-state ^{13}C NMR spectroscopy. *Macromolecules*, *22*, 3892–3898.
Stone, B. A., & Clarke, A. E. (1992). *Chemistry and biology of (1→3)-β-glucans*. Melbourne, Australia: La Trobe University Press.
Stipanovic, A. J., & Giammatteo, P. J. (1987). CP/MAS ^{13}C NMR Studies on aqueous polysaccharide gels. In M. Yalpani (Ed.), *Industrial polysaccharides, genetic engineering, structure/property relations and applications* (pp. 281–292). Amsterdam: Elsevier.
Takeda, H., Yasuoka, N., Kasai, N., & Harada, T. (1978). X-ray structural studies of (1→3)-β-D-glucan (curdlan). *Polymer Journal*, *10*, 365–368.
Wada, M. (2002). Lateral thermal expansion of cellulose I and III_I polymorphs. *Journal of Polymer Science Part B: Polymer Physics*, *40*, 1095–1102.
Wada, M., Hori, R., Kim, U. J., & Sasaki, S. (2010). X-ray diffraction study on the thermal expansion behavior of cellulose Iβ and its high-temperature phase. *Polymer Degradation and Stability*, *95*, 1330–1334.
Wada, M., Kwon, G. J., & Nishiyama, Y. (2008). Structure and thermal behavior of a cellulose I-ethylenediamine complex. *Biomacromolecules*, *9*, 2898–2904.
Wada, M., Okano, T., & Sugiyama, J. (1997). Synchrotron-radiated X-ray and neutron diffraction study of native cellulose. *Cellulose*, *4*, 221–232.
Wada, M., & Saito, Y. (2001). Lateral thermal expansion of chitin crystals. *Journal of Polymer Science Part B: Polymer Physics*, *39*, 168–174.
Yanaki, T., Itoh, W., & Tabata, K. (1986). Correlation between the antitumor activity of schizophyllan and its triple helis. *Agricultural and Biological Chemistry*, *50*, 2415–2416.
Zhang, L., Li, X., Xu, X., & Zeng, F. (2005). Correlation between antitumor activity, molecular weight, and conformation of lentinan. *Carbohydrate Research*, *340*, 1515–1521.